Journal of Sustainability Science and Management *eISSN: 2672-7226*
Volume 18 Number 1, January 2023: 70-85

REMOVAL OF CADMIUM IONS VIA THE MAGNETIC BIOCHAR SYNTHESISED FROM SUGARCANE BAGASSE: FACTORS AFFECTING YIELD AND ADSORPTION CAPABILITY

NORAINI MOHAMED NOOR[1]*, EZZAT CHAN ABDULLAH[2], RAIHAN OTHMAN[1] AND MUBARAK MUJAWAR NASIBAB[3]

[1]Science in Engineering Department, Kulliyyah of Engineering, IIUM Gombak, Jalan Gombak, 53100 Kuala Lumpur, Malaysia. [2]Malaysia - Japan International Institute of Technology (MJIIT), Universiti Teknologi Malaysia, Jalan Semarak, 54100 Kuala Lumpur, Malaysia. [3]Petroleum and Chemical Engineering, Faculty of Engineering, Universiti Teknologi Brunei, Bandar Seri Begawan BE1410, Brunei Darussalam.

**Corresponding author: norainimnoor@iium.edu.my*
Submitted final draft: 2 August 2022 *Accepted: 23 August 2022* http://doi.org/10.46754/jssm.2023.01.005

Abstract: The sugarcane bagasse (SCB) was a precursor in synthesising magnetic biochar using a modified single-stage electric muffle furnace to remove Cd^{2+} ions in industrial wastewater. Nickel (II) oxide (NiO_2) was added to boost the efficiency of yield and the removal of heavy metals. The magnetic biochar (MBN3) was optimally synthesised at 500°C for 30 minutes with an IR of 0.4 to evaluate its performance in adsorption capability. Analyses of Field Emission Scanning Electronic Microscopy indicated that pores in the magnetic biochar enlarged after the impregnation and decomposition with an average diameter of 3.2 nm (MBN3) and surface area of 63.5 m^2g^{-1}. The highest removal for Cd^{2+} onto MBN3 was 87.6%, reaching pH 6.0 and an agitation speed of 125 rpm for 60 minutes. The maximum adsorption capacity (q_m) for the adsorption of Cd^{2+} onto MBN3 was 47.9 mgg^{-1}. The adsorbent followed the pseudo-second-order kinetic model and the Langmuir-Freundlich isotherm model with $R^2 = 0.9853$ (Langmuir) and $R^2 = 0.9538$ (Freundlich), suggesting that the surface of MBN3 might be heterogeneous with different classes of active sites, heavy metals were adsorbed on some classes of active sites only, rather than on all active sites.

Keywords: Carbon materials, magnetic materials, adsorption, water remediation, biomass.

Abbreviations:

AAS	-	Atomic Absorption Spectroscopy
BET	-	Brunauer, Emmett and Teller
EDX	-	Elemental Dispersive X-Ray
EDLC	-	Electrical Double Layer Capacitors
EFB	-	Empty Fruit Bunch
FESEM	-	Field Emission Scanning Electron Microscope
FTIR	-	Fourier Transform Infrared
IR	-	Infrared
JCPDS	-	Joint Committee on Powder Diffraction Standards
JOC	-	Jatropha Oil Cake
MBN1	-	Magnetic Biochar Produced from Nickel (II) Chloride, NiCl
MBN2	-	Magnetic Biochar Produced from Nickel (II) Sulfate, $NiSO_4$
MBN3	-	Magnetic Biochar Produced from Nickel (II) Oxide, NiO
NiCl	-	Nickel (II) Chloride
$NiSO_4$	-	Nickel (II) Sulfate
NiO	-	Nickel (II) Oxide
PFO	-	Pseudo-First Order
PSO	-	Pseudo-Second Order
SCB	-	Sugarcane Bagasse
VSM	-	Vibrating Sample Magnetometer
XRD	-	X-Ray Diffraction
$ZnCl_2$	-	Zinc Chloride

Introduction

In Malaysia, nearly 150,000 tons of dried sugarcane bagasse (SCB) are generated annually (Shafie *et al*., 2011). This agricultural waste primarily comprises cellulose, lignin, and other biopolymers with ample hydroxyl and phenolic groups. Modifying these chemicals could generate products with new characteristics (Chakraborty *et al*., 2020) that absorb hydrophilic and hydrophobic materials.

Over the last few decades, cadmium has been found in high amounts in industrial waste. According to WHO, the safe limit of Cd^{2+} in wastewater is 0.003 ppm (Aneyo *et al*., 2016). Metal pollution such as cadmium is a serious problem in Malaysia because several manufacturing businesses, such as metal-finishing, electronic industries, and mining, are currently increasing in the country. Cadmium is a human carcinogen that can cause cancer and death (Engwa *et al*., 2016). Cancer was the leading cause of death in 2012, owing primarily to genetic instability (Ferlay & Colombet, 2019). Aside from that, inhaling excessive doses of cadmium can seriously damage the lungs (Engwa *et al*., 2016). Consuming high quantities of cadmium can also cause stomach pain, leading to diarrhoea and vomiting (Engwa *et al*., 2016). Even at low levels, long-term cadmium exposure can cause lung damage, brittle bones, and renal failure (Engwa *et al*., 2016). As a result, water pollution has increased dramatically, threatening many of the water's beneficial applications. Because of this, water pollution prevention is necessary to ensure that future generations can enjoy a healthy environment.

Numerous ways to extract metals from wastewater can be found in the literature (Saleh *et al.,* 2022). Regarding extraction, adsorption and membrane filtering are two of the most commonly used processes (as well as chemical precipitation). Ion exchange has been used in the chemical industry to remove metals from waste streams. Synthetic organic ion exchange resins are the most common surfactant used for ion exchange (Amphlett *et al.,* 2020). However, these processes suffer several drawbacks, such as high operational cost (Abdel Salam *et al*., 2011), large substance requirements, low removal efficiency, and incomplete removal of metal ions with chemical residual as a by-product that requires further treatment. Other than that, adsorption is commonly advocated to eliminate harmful metal ion contaminants. Removing metals from inorganic effluents with activated carbon is highly recommended due to its high surface area, increased adsorption capacity, easy operation, high efficiency, high profitability, and specific surface reactivity (Manjuladevi *et al.,* 2018; Saleh *et al.,* 2022).

In producing and synthesising magnetic biochar, many factors that may significantly influence the properties of resulting materials must be considered. The magnetic biochar properties can change the production conditions, making the magnetic biochar properties vary correspondingly. Biomass types and pyrolysis conditions (i.e., thermochemical conversion technology, pyrolysis temperature, and residue time) may affect biochar-based adsorption properties and adsorption ability. However, limited information is available about the effects of these factors. In addition, the parameters of different synthesis methods may greatly affect the synthesis efficiency. Understanding the optimum magnetic biochar production conditions and synthesis parameters to produce magnetic biochar-based adsorbents with the best properties is required.

Although improvements and optimisations have been made toward the properties and performance of magnetic biochar, less attention has been paid to producing high-quality and cost-efficient magnetic biochar with a simple synthesis method. Therefore, it is necessary to have specific knowledge of the synthesis, structural, and magnetic properties of magnetic biochar since the quantity and quality of pyrolysis products such as magnetic biochar are significantly influenced by the operating parameters.

Recent advances in biochar science have rekindled interest in synthetically generating biochar with magnetic characteristics, commonly

known as magnetic biochar. Magnetic biochar is charcoal produced by combining biomass with various magnetic modifiers and pyrolysing it at various temperatures, resulting in biochar and the magnetic modifier combination. For removing metal ions from wastewater, stable and insoluble porous matrixes with appropriate active groups can be effective adsorbents, but their expensive cost limits their usage.

In this respect, magnetically modified SCB had long been known as an efficient sorbent for Pb^{2+} and Cd^{2+} ions, largely via ion exchange (Yu *et al*., 2013). In general, this sorbent is known as magnetic biochar in the removal of heavy metallic ions. The magnetic biochar was synthesised from SCB using a modified single-stage electric muffle furnace in this study. The operating pyrolytic parameters were optimised for the carbon yield to evaluate the adsorption potential of Cd^{2+} ions. The synthesised magnetic biochar's surface morphology and structural properties were also characterised. This study would contribute to sustainable development by removing heavy metallic ions from industrial wastewater while disposing of agricultural wastes.

Materials and Methods

Preparation of Adsorbate and Magnetic Biochar

In this study, the stock solution of Cd^{2+} (1,000 mg/L; analytical grade) was procured from Merck and diluted with 1 L distilled water to prepare a stock solution. The stock solution was agitated for three hours with a shaking incubator at (28 ± 2) °C in the dark and wrapped with an aluminium foil to prevent exposure to light.

Meanwhile, the SCB was sun-baked, rigorously washed with distilled water, and desiccated in an oven at 80°C for 48 hours. Subsequently, the SBC was ground with a plant mill and then macerated with a kitchen blender to generate the powdery biomass, desiccated once more in an oven at 100°C for 24 hours. 20 g of dried biomass, designated as raw SCB was blended with 20 ml of nickel (II) oxide (NiO_2) solution. These samples of SCB in NiO_2 were then placed in a thermal agitator at 200 rpm and 30°C for various periods ranging from 30 to 60 minutes with different impregnation ratios (IRs) given by the standard formula below.

$$IR = \frac{W_{NiO_2}}{W_{SCB}} \quad (1)$$

where W_{NiO} = the dry weight of NiO_2 powder (g) and W_{SCB} = raw SCB (g).

The sludge was then filtered and desiccated in an oven at 80°C for 48 hours. The pyrolysis of the raw SCB was performed in a modified Muffle Furnace (model FP-03, WiseTherm) at 400, 450, 500, 550, 600, 650 and 700°C with a heating rate of 25°C/min. The furnace was vacuumed via a suction pump fastened to the syngas effluent. The pyrolytic decomposition generated the magnetic biochar as a black residue. Upon cooling at room temperature, the black magnetic biochar was washed with distilled water until neutral in pH value, sieved to yield MBN3 with an average particle size smaller than 150 µm, and stowed in an airtight plastic container. The yield of magnetic biochar was calculated using Equation 2 below:

$$\text{Yield } (\%) = \frac{W_1}{W_0} \times 100 \quad (2)$$

where W_1 = the dry weight (g) of the final magnetic biochar produced after the impregnation and W_0 = the dry weight of the precursor in the feed pyrolysis.

Besides, the removal of Cd^{2+} ions from the aqueous solution was calculated using Equation 3 below:

$$\text{Removal } (\%) = \frac{C_1}{C_2} \times 100 \quad (3)$$

where C_1 = the concentration of the Cd^{2+} after absorption and C_2 = the concentration of the Cd^{2+} before absorption.

Adsorption Equilibrium, Isotherms and the Characterisation of Magnetic Biochar

The adsorption capacity of heavy metal ions from the mass balance on the sorbate in a system has often been used to estimate the experimental adsorption isotherms. Studies of

batch adsorption for the Cd^{2+} ions was conducted in six experiments with three replicates each at concentrations of 20, 40, 60, 80, 100, 120 and 140 mg/L, diluted from the stock solution (1000 mg/L) of Cd^{2+} ions. All adsorption experiments were carried out in a 250 mL conical flask by adding 0.3 g of MBN3 to 100 mL of Cd^{2+} aqueous solutions (in different concentrations). The initial concentration of the adsorbate and the adsorbent dosage was fixed throughout the batch experiments. The batch adsorption study of the removal of both adsorbates was carried out separately to understand the adsorption capacity of Cd^{2+} ions onto MBN3. The determination of factors affecting the batch adsorption process was investigated by manipulating the agitation speed between 50-200 rpm and contact time between 10-90 minutes. The adsorbents of heavy metal and results were averaged and the adsorption capacity, q_e was calculated as below:

$$q_e(\text{mg g}^{-1}) = \left[\frac{(C_0 - C_e)V}{m}\right] \quad (4)$$

where C_o = the initial adsorbate concentration in solution (mg/L), C_e = the equilibrium adsorbate concentration in solution (mg/L), V = a known volume of heavy metal ions and m = a known mass of dry adsorbent (g).

Meanwhile, the pH values of the adsorbate solutions were set to range between 2 and 10 using 0.1 M solutions of NaOH or HNO_3 and monitored with a pH meter (Seven Easy pH meter S20, Mettler Toledo). Isotherm studies were performed to evaluate the q_e of magnetic biochar in removing heavy metals. Cd^{2+} solutions at various concentrations were prepared from standard solutions and 100 mL of each standard solution was placed into separate conical flasks. Its initial acidity was set to the optimum adsorption pH for the Cd^{2+} solution and added with 0.3 g magnetic biochar. These solutions with known concentrations were designated as standard solutions. The flasks were stirred with a mechanical agitator at room temperature and 160 rpm.

The batch equilibrium data of magnetic biochar in initial Cd^{2+} concentrations (20 - 140 mg/L) were fitted by Langmuir and Freundlich isotherm models, which were calculated using Equation 5 and Equation 6 below.

$$q_e = q_{max}\frac{K_L C_e}{1 + K_L C_e} \quad (5)$$

where q_e = the adsorption capacity at equilibrium (mg/g), q_{max} = the theoretical maximum adsorption capacity of the adsorbent (mg/g), K_L = the Langmuir affinity constant (L/mg) and C_e = the supernatant equilibrium concentration of the system (mg/L).

$$q_e = K_F C_e^{1/n} \quad (6)$$

where K_F = the Freundlich constant related to the adsorption capacity, q_e (mg/g) and n = the heterogeneity coefficient (dimensionless).

After three hours, the content of each flask was filtered, and the metal contents of the filtrate were determined using an Atomic Absorption Spectrometer (Perkin Elmer Analyst 400). Meanwhile, the crystalline structure of the magnetic biochar (MBN3) used to absorb the heavy metal was characterised using an X-ray Diffractometer with CuKα radiation (XRD-6000, Shimadzu), and its Field Emission Scanning Electronic Microscopy (FESEM) with energy dispersive X-ray spectroscopy (EDX) was examined using a Scanning Electronic Microscope (Supra 35VP. ZEISS). Besides, the infrared spectrum of the function groups was assayed using a Fourier Transform-Infrared spectrophotometer (FT-IR, Nicolet Smart i-s10, Thermo Sci). Brunauer–Emmett–Teller (BET). Finally, we selected the best MBN3 produced at optimum parameters and tested its magnetic properties using Vibrating Sample Magnetometer (VSM).

Results and Discussion

Effects of Pyrolytic Temperature, Time and Impregnation Ratio

Figure 1 (a) shows the effects of pyrolytic temperature on the yield of magnetic biochar, in which 400°C gave the highest yield, i.e., 42.5%, and 700°C produced the lowest yield (21.2%). In general, the yield decreased as the

temperature increased. In particular, when the temperature increased from 400 to 600°C, the yields decreased by nearly 50% of the initial value, suggesting that most volatile matters in SCB might have been disintegrated at higher temperatures, leaving behind a small amount of magnetic biochar with high carbon content. In contrast, slow heating gave the volatile matter a long time to disintegrate, forming more surface pores (Yu *et al*., 2013). Meanwhile, the highest yield of magnetic biochar for MBN3 (42.5%) occurred at 400°C and 450°C, probably at lower temperatures, the volatile matter decomposed slower.

In general, the yield of magnetic biochar synthesised by different concentrations of NiO_2 solutions differed slightly. The activation energy required to manifest the magnetic properties differs among metals, and thermo-chemically metallic ions would vary in the conversion efficiency for the formation of char as well as in catalysing secondary reactions such as rearrangement reactions in the cellulosic matrix that give higher stability of the polymer through a higher degree of reticulation (Yu *et al*., 2013). However, in the presence of nickel, the yield of magnetic biochar decreased from 42.5 to 21.2%, probably because of a higher emission of H_2 (Foo & Hameed, 2012a).

Besides, Figure 1 (a) shows that when the temperature of MBN3 increased from 400 to 500°C, the removal also increased from 87.4 to 88.6%. Beyond 500°C the removal began to dwindle with the increment of temperature, probably due to insufficient pore structures and active sites at high pyrolytic temperatures (Peng *et al.,* 2019). In particular, over-gasification would occur at 700°C, thereby decreasing the porosity and surface area. Consequently, both the yield of magnetic biochar and removal efficiency dwindled gradually. In contrast, at temperatures below 500°C, the removal of adsorbent progressively increased.

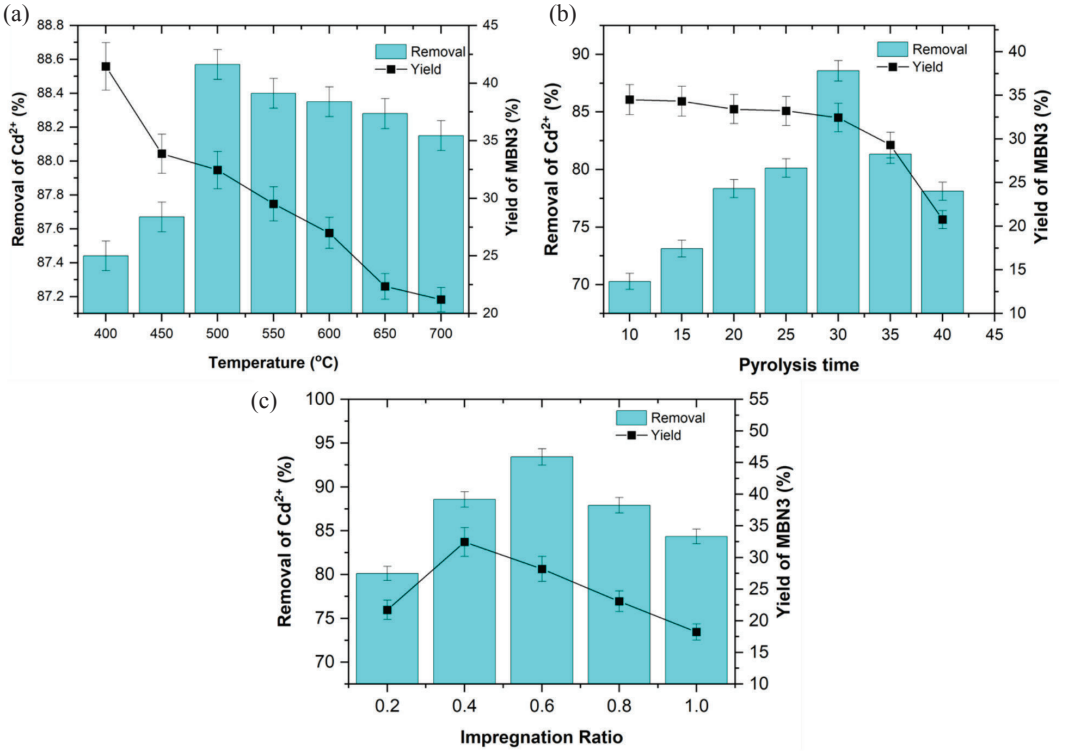

Figure 1: Yields of magnetic biochar and cadmium removal after slow pyrolysis of MBN3 at different parameters: (a) Temperature, (b) Pyrolysis time and (c) Impregnation ratio

Figure 1 (b) shows the effects of pyrolytic time on the yield of magnetic biochar, in which the highest yield, i.e., 34.7% was attained at 10 minutes and the lowest yield (20.7%) at 40 minutes. In general, the yield of magnetic biochar formed a linear relationship with the pyrolytic time from 10 to 30 minutes, beyond which the yield began to decline. Longer exposure to high temperatures (> 700°C) would induce the reactions of C-NiO_2 and C-CO_2 reactions, thereby expediting the disintegration of the C-O-C and C-C bonds (Collard *et al*., 2012).

Since the maximum yield was attained at the pyrolytic time of 30 minutes, prolonging the pyrolytic time would accelerate the reaction rate and devolatilisation, thereby facilitating the development of porosity (Yu *et al*., 2013) and the formation of active sites within the magnetic biochar (Unugul & Nigiz, 2020) for higher absorption of metallic ions. A slight decrease in yield occurred at 30 minutes, suggesting that as the energy activation progressed, the dehydration and disintegration of active sites within the magnetic biochar intensified (Andas *et al.,* 2017). Incorporating NiO_2, which acted as an activating agent, facilitated the depolymerisation, dehydration, and redistribution of the constituent biopolymers while transforming the aliphatic into aromatic compounds (Bag *et al.,* 2020).

In contrast, extending the pyrolytic time from 10 to 30 minutes drastically improved the removal efficiency from 70.3 to 87.6% for MBN3, suggesting that increasing the exposure time would increase the reaction rates, thus developing the essentials of the pore structure (Foo & Hameed, 2012b). However, by increasing the pyrolytic time from 30 to 40 minutes, the removal efficiency of MBN3 decreased from 87.6 to 78.1%, probably because more carbon of the pores was burnt. Figure 1 (c) shows the yield of MBN3 and the removal percentage of Cd^{2+} ions by magnetic biochar at different IRs, in which the highest removal, i.e., 94.5% was attained at the IR of 0.6 and the lowest removal (74%) at 1.0. In general, the IR was linearly related to the yield of magnetic biochar. Specifically, as IR increased from 0.2 to 0.4, the yield of magnetic biochar increased from 21.7 to 32.5%, probably due to the detraction of gases such as H_2 which resulted in a higher yield of magnetic biochar (Abioye & Ani, 2017). Also, the ratio of impregnated metal might occupy larger void areas and hence a higher yield of magnetic biochar. When the optimum IR was reached, the excessively impregnated metal might also facilitate vigorous gasification, thereby destroying the carbon framework while resulting in a drastic reduction of accessible area and burning of pores and hence, a decline of removal efficiency (Foo & Hameed, 2012b).

Similarly, as the IR increased from 0.2 to 0.6, the removal efficiency increased from 80.1 to 93.4%, after which it dwindled gradually. As the IR increased, more metallic ions would cross-link with the functional groups on the surface of the biomass due to the rapid diffusion of the metallic ions in the bulk solution and the shortening of the distance between the metals and ligands (Andas *et al.,* 2017) from decomposition and leaching. Such crosslinking would generate high surface areas and pore volumes in the magnetic biochar, thereby enhancing the removal efficiency of heavy metal ions. Beyond the optimum IR (0.6), the excessively impregnated metal would block the pores, thereby reducing the accessible area (Sun *et al*., 2011).

Characterisation of Magnetic Biochar

Figure 2 shows the FESEM images of the raw SCB, SCB biochar, and MBN3 with an irregular smooth structure within the non-uniform parallel layer of SCB [(Figure 2 (a)] and large-sized pores (50 μm) in its morphology [(Figure 2 (b)]. Another study (Tungal *et al.,* 2011) also found large pores. The enlargement of pores was indicative of other materials, such as the dissolution of lignin and other constituents from the sugarcane bagasse during the impregnation. The release of volatile constituents from the particle escalated progressively when the final temperature increased during the heating. Figure 2 (c-d) shows that macropores of various sizes and shapes were developed with some agglomerations at the optimum condition. The

elemental analysis on the surface of MBN3 [Figure 2 (e)] shows the presence of C, N, O, Ni and Cd was confirmed. The additional line of Ni Kα at 0.85 keV was detected as a result of the successful binding of the metal salts during impregnation.

Figure 3 (a) shows the XRD patterns for the SCB biochar and MBN3 at optimum conditions, in which the NiO-SCB disintegrated at 500°C with the formation of cubic nickel oxide (JCPDS no. 47-1049) and amorphous carbon. By lengthening the pyrolytic time, the carbon reduced the nickel complex to the metallic nickel (JCPDS no. 87-0712) at a very minimal oxygen environment (Foo & Hameed, 2012c). Incidentally, a very weak (002) and broad diffraction peak of graphitic carbon (JCPDS no. 75-1621) was identified, indicating a low graphitisation of carbon in MBN3. The reduction of NiO_2 to Ni^0 between 400 to 500°C was probably due to the biochar, which might serve as a reducing agent.

Figure 3 (b) shows the FT-IR spectra of raw SCB and MBN3. Asymmetric absorption bands were detected at 3495 cm^{-1} for raw SCB and MBN3, indicating the occurrence of exchangeable OH^- groups. The C–H stretching of non-ionic carboxylic groups was detected at

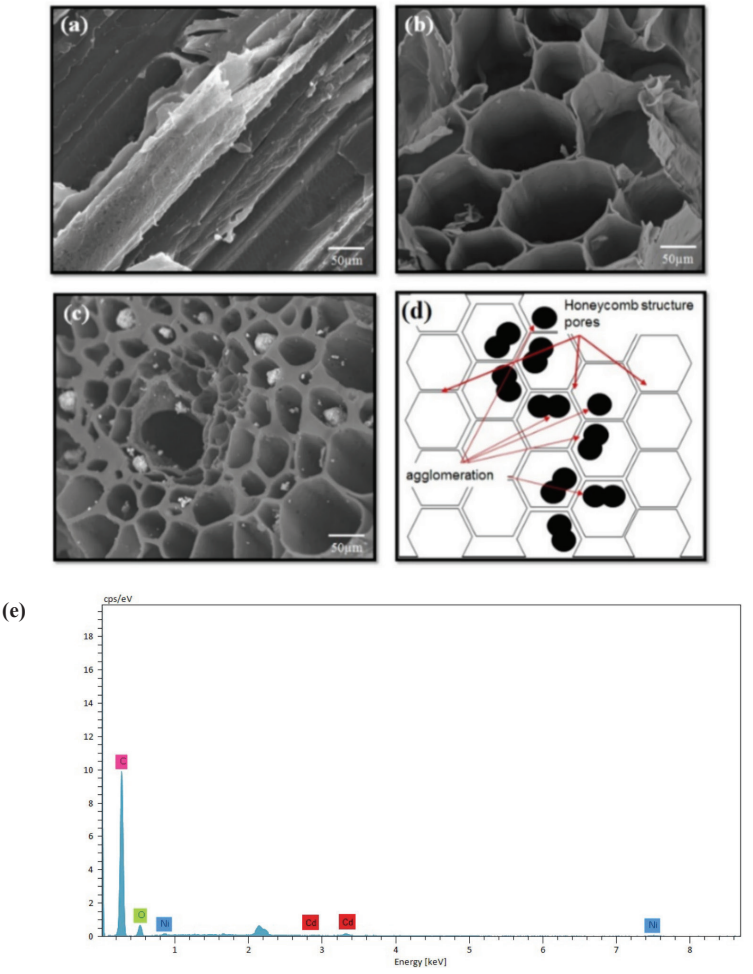

Figure 2: The FESEM images of the raw SCB, SCB biochar and MBN3: (a) The irregular smooth structure within the non-uniform parallel layer of SCB, (b) Large-sized pores, (c-d) Macropores with various sizes and shapes with some agglomerations and (e) Elemental analysis of MBN3 after adsorption of cadmium

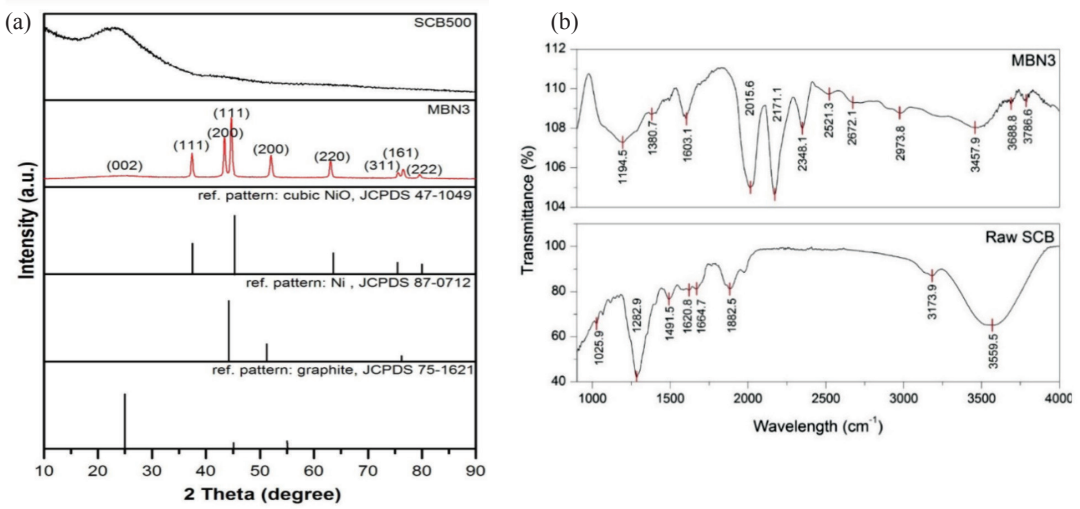

Figure 3: (a) The XRD patterns for the SCB biochar and MBN3 at optimum condition and (b) FT-IR spectra of the raw SCB and MBN3

2750 cm^{-1} and 3000 $cm^{-1,}$ while peaks at 1700 cm^{-1} were attributable to the asymmetric and symmetric stretching vibration of C=O bond in ionic carboxylic groups of –COO–. Besides, the peak at 1245 cm^{-1} was attributable to the C-O-C in lignin.

Overall, peaks at 1200 cm^{-1} in MBN3 were more intensive than that of SCB500, probably due to the vanishing of ester bond stretching. Specifically, the decomposition damaged the ester bond linkage between the carbohydrate and lignin, releasing the cellulose from lignin encapsulation and causing more exposition of the cellulose. Moreover, the shifting of peaks indicated the presence of metal particles on the surface of magnetic biochar, accounting for the functional groups of MBN3 that participated in the complexation with both metal particles (Moubarik & Grimi, 2014). In agreement with FTIR spectra, it is suggested that the mechanism of Cd^{2+} adsorption onto MBN3 was related to surface complexation (Figure 4).

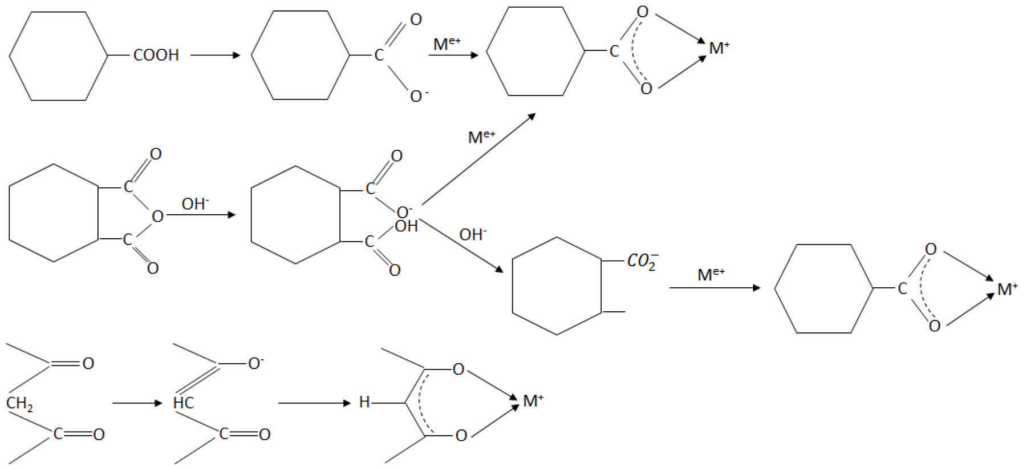

Figure 4: Proposed mechanism of Cd^{2+} sorption on MBN3

Table 1 shows the best Brunauer–Emmett–Teller (BET) surface area and pore volume of the magnetic biochar as type IV, indicating that the MBN3 can be categorised as mesoporous materials. Overall, the surface areas and pore volumes increased upon thermos-chemical modification. Specifically, the raw SCB had a smooth surface, and the pyrolysis caused the formation of pores on the surface structure. It was believed that the impregnating NiO_2 of the biomass, which simultaneously affected the surface area, caused the generation of pores (Wang *et al*., 2013). The substantial enhancement in the surface area and pore volume of magnetic biochar might be due to the substantial increment in the emission of volatiles (Yu *et al.*, 2013). Since the pyrolytic temperature of developing MBN3 was high, the remainder of raw SCB was fully disintegrated, further enhancing the production of highly ordered aromatic structures of magnetic biochar.

The sample showed ferromagnetic properties, revealed by the coercive field of 251.51 Oe and the saturation magnetisation of 7.4981 emu/g. The saturation magnetisation of MBN3 may be due to the larger number of nickel oxide particles in MBN3. It shows that the magnetisation process of the biochar was successful. Such behaviour was expected due to the decreased degree of orientation of the magnetic moments with the increasing temperature as MBN3 was produced at high temperatures (Li *et al*., 2017). Hysteresis loops of MBN3 (Figure 5) indicated that the magnetic biochars are ferromagnetic materials due to the non-linear curve of M – H, and the magnetisation saturates at higher values of H (Zhang *et al*., 2013).

Table 1: Textural characteristics of raw SCB and magnetic biochar

Typical Properties	Raw SCB	MBN3
Specific surface area (m^2/g)	1.806	63.513
Micropore surface area (m^2/g)	*	44.798
Total pore volume (cm^3/g)	0.001	0.052
Average pore diameter (nm)	2.333	3.227

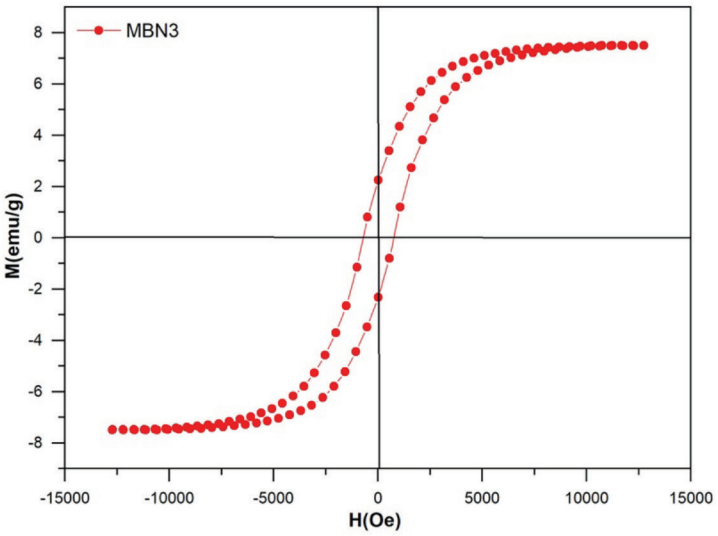

Figure 5: Magnetic hysteresis loop of MBN3 produced at optimum condition

Effects of Initial Concentration, Contact Time and pH on the Adsorption Equilibrium, Isotherm and Kinetics

Figure 6 (a) shows the effects of pH on the adsorption of Cd^{2+} ions led by MBN3, in which the removal efficiency for cadmium attained a maximum of 97% at pH 6. The removal efficiency increased linearly with pH values. However, as pH values increased beyond six, the removal efficiency declined. At lower pH, H^+ and Cd^{2+} ions adsorbed competitively for adsorption sites, causing the removal efficiency to dwindle. The adsorption of Cd^{2+} ions showed the lowest value of 87.7% for MBN3 at pH 2. The pH_{pzc} value of 8.7 was obtained for MBN3 [(Figure 5 (c)] might be due to the pyrolysis temperature, which produced some amount of ash content (Tan *et al*., 2014) and the release of alkali salts from the pyrolytic structure at higher pyrolysis temperature (Chen *et al*., 2011b). At higher temperatures, the amounts of negatively charged functional groups on biochars (e.g., –COO^-, –COH, and –OH) were reduced, resulting in fewer negative surface charges and increased pH_{pzc} (Li *et al*., 2017b).

At a pH value lower than pH_{pzc}, the surface of the magnetic biochar is positively charged where the H^+ ions reside on the surface rather

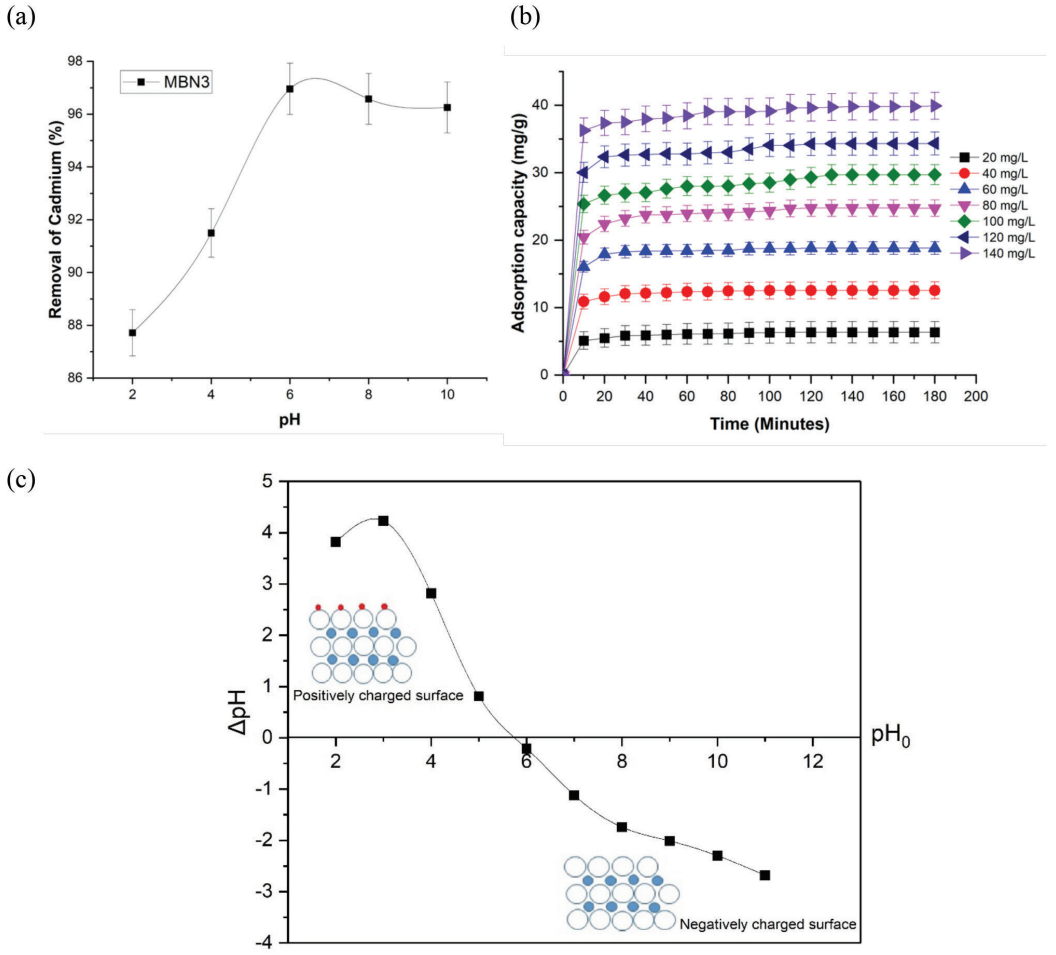

Figure 6: (a) The effects of pH on the adsorption of Cd^{2+} ions led by MBN3 over a pH range of 2-10 at 25°C with an agitation speed of 75 rpm, (b) Adsorption capacity (q_t) versus contact time (t) of Cadmium with a different concentration on MBN3 and (c) Curve of the point of zero charges (pH_{pzc}) for MBN3

then entering the solution which reduces the magnetic biochar molecules bound on the sorbent surface due to high electrostatic repelling forces which inhibits the contact of cation species and the magnetic biochar surface (Wu *et al.,* 2021). On the other hand, the surface of the magnetic biochar is negatively charged, containing unshared electron pairs on the magnetic biochar surface and cationic metal ions in a solution at a pH value higher than pH_{pzc} (Wu *et al.,* 2021). Thus, the adsorption of metal ions was favoured at a pH value slightly higher than pH_{pzc} due to the increasing electrostatic attraction between cations species and magnetic biochar particles.

Figure 6 (b) shows the q_e (mg/g) of MBN3 through time for the adsorption of Cd^{2+} ions at various concentrations, in which the highest q_e, i.e., 40 mg/g, occurred at 140 mg/L concentration, and the lowest at 5 mg/g and 20 mg/L, respectively. The q_e was linearly related to the initial concentration of the metal ions. Adsorption of high initial Cd^{2+} concentration caused the q_e to increase due to the mass-transfer driving force incrementing a higher adsorption rate (Mubarak *et al*., 2014). Also, the adsorption escalated as the contact time lengthened until the attainment of an equilibrium, where the adsorption rate levelled off over time as the surface of the adsorbent became saturated with metal ions. The initial adsorption rate was high, probably due to a large ratio of the surface area of the adsorbent and ions. This ratio levelled off as time elapsed due to slower dissemination of the adsorbate into the core of the adsorbent.

Figure 6 (c) also shows the absorption kinetics of Cd^{2+} ions via magnetic biochar, which occurred rapidly in the first 10 minutes, slowing down until the equilibrium was achieved. The swift mass transfer of energy on the outer surface of the adsorbent seemed to be responsible for the initial rapid adsorption followed by a slower internal diffusion (Wang *et al*., 2016). Initially, the active sites on the surface of the sorbent were largely empty. As time elapsed, the heavy metal ions gradually occupied the active sites, thereby slowing down the sorption rate (Bag, Tekin & Karagoz, 2020). At 40 minutes, the sorption system nearly achieved equilibrium.

Table 2 shows the isotherm parameters for the adsorption of Cd^{2+} ions onto MBN3. Meanwhile, Figure 7 shows plots of linearised Langmuir [Figure 7 (a)] and Freundlich [Figure 7 (b)] isotherms, in which the Cd^{2+} adsorption fit the Langmuir (R^2 = 0.9853) better than Freundlich (R^2 = 0.9538) isotherm. Hence, the adsorption of Cd^{2+} ions onto MBN3 followed the Langmuir model, i.e., the uptake occurred on a homogenous surface via monolayer sorption with equivalent sites (Ding *et al*., 2012), and the adsorption capability of a molecule at a given site was independent on the occupation. However, the Langmuir isotherm showed that the Cd^{2+} ions could be adsorbed on all classes of active sites, i.e., the surface of magnetic biochar was homogenous for Cd^{2+} adsorption. Based on the R^2 value, the Cd^{2+} adsorption might also fit the Freundlich isotherm, suggesting that the surface of MBN3 might be heterogeneous with different classes of active sites. Heavy metals were adsorbed on only some classes of active sites rather than on all active sites.

Figure 8 shows the FT-IR spectra for the adsorption of Cd^{2+} onto the magnetic biochar with a few functional groups on the surface of the magnetic biochar before the adsorption of Cd^{2+} (labelled as MBN3), but more peaks were detected after the adsorption (labelled as MBN3-Cd). Alterations in the peak position after heavy metal adsorption might be attributable to the adherence of heavy metal ions via electrostatic binding. FT-IR spectra of MBN3 and MBN3-Cd (Figure 8) indicated an apparent shift of position for the characteristic peak of MBN3 from 3457.6 cm^{-1} (O-H stretching) to 3480.2 cm^{-1}, suggesting that hydroxyl groups interacted with metal cations on MBN3 during the adsorption (Grassi *et al*., 2012). Together, distinct changes before and after the absorption in peak frequencies of OH, C-O stretch in acids, C-O stretch in phenols, and C-O-C stretch in ethers suggested that these ionisable functional groups on the adsorbent surface could bind with metal ions. These changes agreed with Langmuir isotherm (Gupta & Nayak, 2012).

Table 2: The isotherm parameters for the adsorption of Cd^{2+} ions onto MBN3

Langmuir Isotherm Model			Freundlich Isotherm Model		
q_{max} (mgg^{-1})	K_L (lmg^{-1})	R^2	K_F		R^2
47.85	0.1962	0.9853	8.7837	0.5356	0.9538

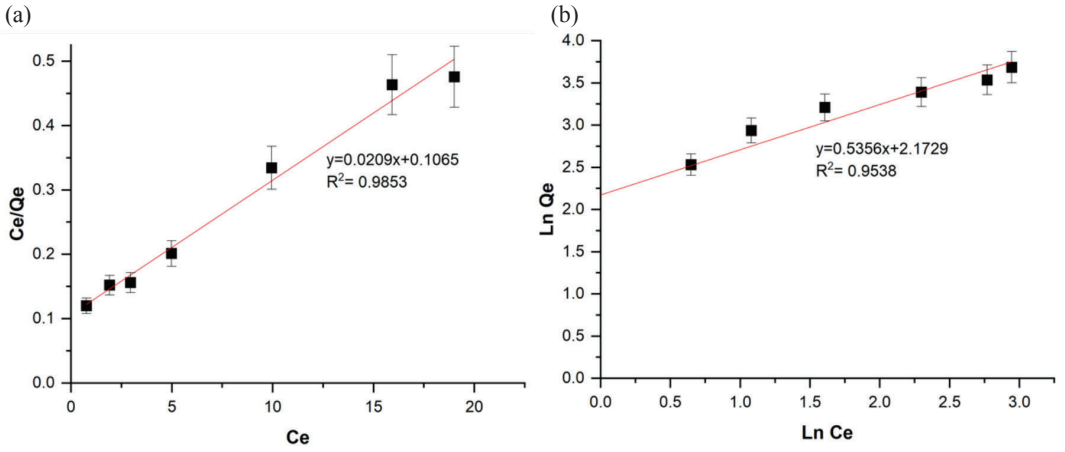

Figure 7: Plots of linearised isotherms: (a) Langmuir isotherm and (b) Freundlich isotherm

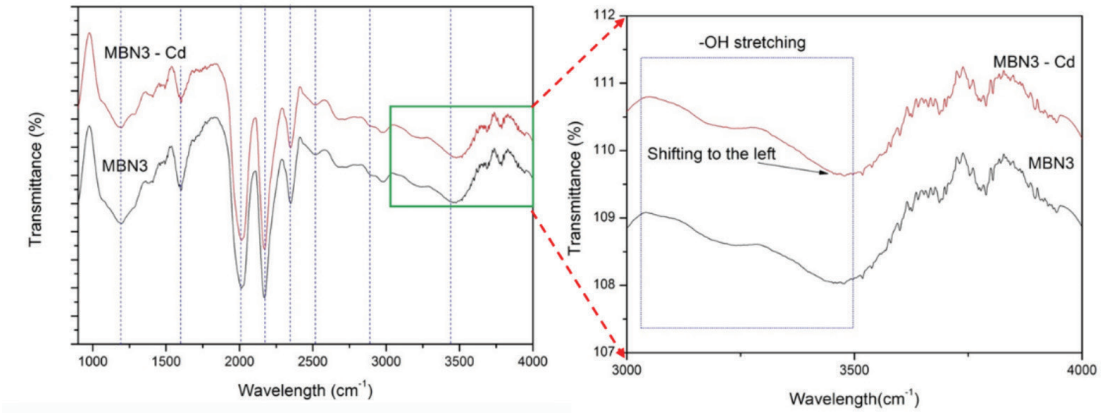

Figure 8: The FT-IR spectra before and after the adsorption of Cd^{2+} onto the magnetic biochar

Table 3 shows the adsorption fitted with kinetic models, including the pseudo-first-order, pseudo-second-order, and intra-particle diffusion models with their respective values of R^2. The adsorption of Cd^{2+} ions on MBN3 followed the pseudo-second-order kinetics model with an R^2 of 0.9999. Also, the R^2 for the adsorption of Cd^{2+} ions did not differ significantly from that of the pseudo-second-order. A pseudo-second-order model suggested that chemical reactions, such as the exchange of cations, complexation, and precipitation, might be responsible for the adsorption (Wang *et al*., 2016). Meanwhile, the intra-particle diffusion model did not fit the data well with a relatively lower correlation coefficient ($R^2 < 0.93$).

Figure 9 shows the XRD patterns of MBN3 before (labelled as MBN3) and after the adsorption of Cd^{2+} (labelled as MBN3-Cd), and the peak at $2\theta = 43.1°$ for MBN3 indicated the

Table 3: The adsorption fitted with kinetic models, including the pseudo-first order, pseudo-second order and intra-particle diffusion model

C_0	q_{ex} (mg/g)	Pseudo First-order Model			Pseudo Second-order Model			Intraparticle Diffusion Model		
Cd^{2+}		k_1 (1/min)	q_e (mg/g)	R^2	k_2 (g/mg·min)	q_2 (mgg^{-1})	R^2	K_i (g/mg·$min^{1/2}$)	C (mgg^{-1})	R^2
20	6.42	-0.0566	2.57	0.8671	0.2889	6.49	0.9999	0.1008	5.18	0.8119
40	12.69	-0.0614	2.62	0.9304	0.5873	12.71	0.9999	0.1202	11.2	0.7082
60	18.93	-0.0561	3.28	0.8923	0.6559	19.01	0.9999	0.1656	16.94	0.5712
80	24.91	-0.0554	1.14	0.7529	0.3632	25.19	0.9999	0.3157	21.08	0.7595
100	29.7	-0.0457	1.36	0.7821	0.2211	30.4	0.9993	0.4147	24.56	0.9607
120	34.27	-0.0477	1.89	0.8935	0.3757	34.84	0.9998	0.3358	30.28	0.8376
140	39.64	-0.0413	1.91	0.9551	0.4359	40.32	0.9999	0.3364	35.78	0.9385

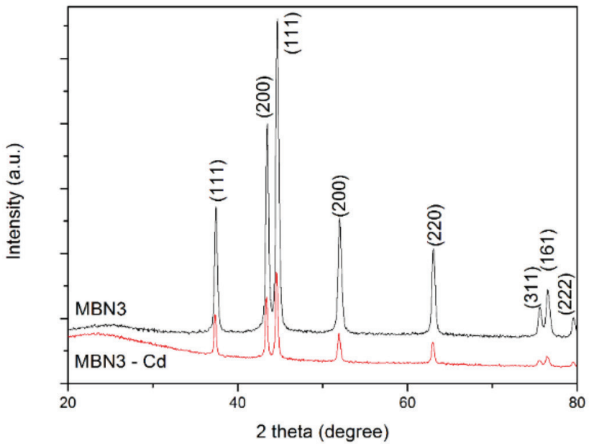

Figure 9: The XRD pattern before and after the adsorption of Cd^{2+}

binding of a large amount of nickel and NiO_2 on the biochar. However, peak intensities dwindled afterward, suggesting that the adsorption of Cd^{2+} eroded the lattice structure of the magnetic biochar, probably via the demolition of hydrogen bonding (Lu *et al*., 2012). Besides, the lattice strain within the structure might decrease the peak intensities of MBN3 after Cd^{2+} adsorption (Cullity, 1956). This XRD pattern was consistent with FT-IR spectra, suggesting that the adsorption of Cd^{2+} onto MBN3 was related to the surface complexation of active functional groups, inner-sphere complexation, surface precipitation, electrostatic attraction, and physical adsorption in which the Cd^{2+} ions were attached either directly to the surface of magnetic biochar, or to the active functional groups that were on the surface of magnetic biochar.

Conclusion

This study investigated the synthesis and characterisation of magnetic biochar generated from SCBC to adsorb heavy metal ions, and the performance of MBN3 as an adsorbent was also evaluated. The highest adsorption for Cd^{2+} ions onto MBN3 was attained at 25°C with an optimal pH of 6.0. The adsorption obeyed the pseudo-second-order kinetic model, suggesting the occurrence of chemisorption. A Langmuir-Freundlich isotherm model explained the

surface of MBN3 might be heterogeneous with different classes of active sites. Heavy metals were adsorbed on only some classes of active sites rather than on all active sites. The maximum adsorption capacities (q_m) for Cd^{2+} ions were higher than that of Cd^{2+} ions onto raw SCB (0.955 mg/g), i.e., SCB was more efficient in generating magnetic biochar. Besides, NiO_2 was a potential transition metallic salt for impregnation in synthesising magnetic biochar to remove heavy metals. As a suggestion, further research on the effects of various metal impregnations could be done and the focus on another adsorption model could be considered.

Acknowledgements

The authors would like to thank the International Islamic University Malaysia for funding this research under IIUM Research Acculturation Grant Scheme (IRAGS), IRAGS18-021-0022.

References

Abioye, A. M., & Ani, F. N. (2017). Advancement in the production of activated carbon from biomass using microwave heating. *Jurnal Teknologi*, *79*(3), 79-88. https://doi.org/10.11113/jt.v79.7249

Amphlett, J. T., Choi, S., Parry, S. A., Moon, E. M., Sharrad, C. A., & Ogden, M. D. (2020). Insights on uranium uptake mechanisms by ion exchange resins with chelating functionalities: Chelation vs. anion exchange. *Chemical Engineering Journal*, *392*, 123712.

Andas, J., Rahman, M. L. A., & Yahya, M. S. M. (2017). Preparation and characterization of activated carbon from palm kernel shell. *IOP Conference Series: Materials Science and Engineering, 226*(1), 012156. https://iopscience.iop.org/article/10.1088/1757-899X/226/1/012156/pdf

Aneyo, I. A., Doherty, F. V., Adebesin, O. A., & Hammed, M. O. (2016). Biodegradation of pollutants in wastewater from pharmaceutical, textile and local dye effluent in Lagos, Nigeria. *Journal of Health and Pollution*, *6*(12), 34-42. https://doi.org/10.5696/2156-9614-6.12.34

Bag, O., Tekin, K., & Karagoz, S. (2020). Microporous activated carbons from lignocellulosic biomass by KOH activation. *Fullerenes, Nanotubes and Carbon Nanostructures*, *28*(12), 1030-1037. https://doi.org/10.1080/1536383X.2020.1794850

Chakraborty, R., Asthana, A., Singh, A. K., Jain, B., & Susan, A. B. H. (2022). Adsorption of heavy metal ions by various low-cost adsorbents: A review. *International Journal of Environmental Analytical Chemistry*, *102*(2), 342-379. https://doi.org/10.1080/03067319.2020.1722811

Chen, T., Zhou, Z., Han, R., Meng, R., Wang, H., & Lu, W. (2015). Adsorption of cadmium by biochar derived from municipal sewage sludge: Impact factors and adsorption mechanism. *Chemosphere, 134*, 286–293. https://doi.org/10.1016/j.chemosphere.2015.04.052

Collard, F. X., Blin, J., Bensakhria, A., & Valette, J. (2012). Influence of impregnated metal on the pyrolysis conversion of biomass constituents. *Journal of Analytical Applied Pyrolysis*, *95*, 213–226. https://doi.org/10.1016/j.jaap.2012.02.009

Cullity, B. D. (1956). *Elements of X-ray diffraction* (2nd ed.). Addison-Wesley Publishing Company, Inc.

Ding, Y., Jing, D., Gong, H., Zhou, L., & Yang, X. (2012). Biosorption of aquatic cadmium (II) by unmodified rice straw. *Bioresources Technology*, *114*, 20–25.

Engwa, G. A., Ferdinand, P. U., Nwalo, F. N., & Unachukwu, M. N. (2019). Mechanism and health effects of heavy metal toxicity in humans. In Karcıoğlu, Ö. & B. Arslan (Eds.), *Poisoning in the modern world-new tricks for an old dog*? IntechOpen. https://doi.org/10.5772/intechopen.82511

Ferlay, J., & Colombet, M. Soerjomataram I, Mathers C, Parkin, D.M, Piñeros M, & Znaor A, Bray F. (2019). Estimating the global cancer incidence and mortality in 2018: GLOBOCON sources and methods. *International Journal of Cancer*, *144*(8), 1941-1953. https://doi.org/10.1002/ijc.31937

Foo, K. Y., & Hameed, B. H. (2012a). Mesoporous activated carbon from wood sawdust by K_2CO_3 activation using microwave heating. *Bioresources Technology*, *111*, 425-432. https://doi.org/10.1016/j.biortech.2012.01.141

Foo, K. Y., & Hameed, B. H. (2012b). Preparation, characterization and evaluation of adsorptive properties of orange peel-based activated carbon via microwave-induced K_2CO_3 activation. *Bioresources Technology* 104, 679–686. https://doi.org/10.1016/j.biortech.2011.10.005

Foo, K.Y., Hameed, B.H. (2012c). Coconut husk derived activated carbon via microwave-induced activation: Effects of activation agents, preparation parameters and adsorption performance. *Chemical Engineering Journal*, *184*, 57-65.

Grassi, M., Kaykioglu, G., Belgiorno, V., & Lofrano, G. (2012). Removal of emerging contaminants from water and wastewater by adsorption process. In Lofrano, G. (Eds.), *Emerging Compounds Removal from Wastewater Natural and Solar Based Treatments* (pp. 15–37). Netherlands: Springer. https://doi.org/10.1007/978-94-007-3916-1_2

Gupta, V. K., & Nayak, A. (2012). Cadmium removal and recovery from aqueous solutions by novel adsorbents prepared from orange peel and Fe_2O_3 nanoparticles. *Chemical Engineering Journal*, *180*, 81–90. https://doi.org/10.1016/j.cej.2011.11.006

Li, H., Awadh, S., Mahyoub, A., Liao, W., Xia, S., Zhao, H., & Guo, M. (2017a). Effect of pyrolysis temperature on characteristics and aromatic contaminants adsorption behavior of magnetic biochar derived from pyrolysis oil distillation residue. *Bioresources Technology*, *223*, 20-26. https://doi.org/10.1016/j.biortech.2016.10.033

Li, H., Dong, X., da Silva, E. B., de Oliveira, L. M., Chen, Y., & Ma, L. Q. (2017b). Mechanisms of metal sorption by biochars: Biochar characteristics and modifications. *Chemosphere* 178, 466–478. https://doi.org/10.1016/j.chemosphere.2017.03.072

Lu, H., Zhang, W., Yang, Y., Huang, X., Wang, S., & Qiu, R. (2012). Relative distribution of pb^{2+} sorption mechanisms by sludge-derived biochar. *Water Research*, *46*, 854–862.

Manjuladevi, M., Anitha, R., & Manonmani, S. (2018). Kinetic study on adsorption of Cr (VI), Ni (II), Cd (II) and Pb (II) ions from aqueous solutions using activated carbon prepared from Cucumis melo peel. *Applied Water Science*, *8*(1), 1-8.

Moubarik, A., & Grimi, N. (2014). Valorization of olive stone and sugarcane bagasse by-products as bio sorbents for the removal of cadmium from aqueous solution. *Food Research International, 73*, 169–175.

Mubarak, N. M., Kundu, A., Sahu, J. N., Abdullah, E. C., & Jayakumar, N. S. (2014). Synthesis of palm oil empty fruit bunch magnetic pyrolytic char impregnating with $FeCl_3$ by microwave heating technique. *Biomass and Bioenergy, 61*, 265–275.

Peng, J., Liu, X., & Bao, Z. (2019). Pyrolysis behaviour of basswood by TG. In *IOP Conference Series: Materials Science and Engineering, 490*(2), 022051.

Richardson, Y., Motuzas, J., Julbe, A., Volle, G., & Blin, J. (2013). Catalytic investigation of in situ generated Ni metal nanoparticles for tar conversion during biomass pyrolysis. *The Journal of Physical Chemistry C, 117*, 23812–23831. https://doi.org/10.1021/jp408191p

Saleh, T. A., Mustaqeem, T., & Khaled, M. (2022). Water treatment technologies in

removing heavy metal ions from wastewater: A review. *Environmental Nanotechnology, Monitoring & Management, 17*, 100617.

Saleh, T. A., Sarı, A. & Tuzen, M. (2022). Simultaneous removal of polyaromatic hydrocarbons from water using polymer modified carbon. *Biomass Conversion and Biorefinery*. https://doi.org/10.1007/s13399-021-02163-9

Shafie, S. M., Mahlia, T. M. I., Masjuki, H. H., Andriyana, A. (2011). Current energy usage and sustainable energy in Malaysia: A Review. *Renewable & Sustainable Energy Reviews*, *15*(9), 4370–4377. https://doi.org/10.1016/j.rser.2011.07.113

Sun, K., Ro, K., Guo, M., Novak, J., Mashayekhi, H., & Xing, B. (2011). Sorption of bisphenol A, 17α-ethinyl estradiol and phenanthrene on thermally and hydrothermally produced biochars. *Bioresources Technology*, *102*, 5757–5763. https://doi.org/10.1016/j.biortech.2011.03.038

Tan, C., Yaxin, Z., Hongtao, W., Wenjing, L., Zeyu, Z., Yuancheng, Z., & Lulu, R. (2014). Influence of pyrolysis temperature on characteristics and heavy metal adsorptive performance of biochar derived from municipal sewage sludge. *Bioresources Technology*, *164*, 47–54. https://doi.org/10.1016/j.biortech.2014.04.048

Tungal, R., Shende, R. V, & Christopher, L. P. (2011). Nickel catalyzed high-pressure hydrothermal processing of biomass for H_2 production. *Journal of Energy and Power Engineering*, *5*, 504–514. https://doi.org/10.1016/j.biortech.2014.04.048

Unugul, T., & Nigiz, F. U. (2020). Preparation and characterization of an active carbon adsorbent from waste mandarin peel and determination of adsorption behaviour on the removal of synthetic dye solutions. *Water, Air, & Soil Pollution*, *231*(11), 1-14.

Wang, Y., Wang, X., Wang, X., Liu, M., Wu, Z., Yang, L., Xia, S., & Zhao, J. (2013). Adsorption of Pb (II) from aqueous solution to Ni-doped bamboo charcoal. *Journal of Industrial and Engineering Chemistry, 19*, 353–359.

Wang, Z., Han, L., Sun, K., Jin, J., Ro, K. S., Libra, J. A., Liu, X., & Xing, B. (2016). Sorption of four hydrophobic organic contaminants by biochar's derived from maize straw, wood dust and swine manure at different pyrolytic temperatures. *Chemosphere*, *144*, 285-291. https://doi.org/10.1016/j.chemosphere.2015.08.042

Wang, Z., Liu, G., Zheng, H., Li, F., Ngo, H. H., Guo, W., Liu, C., Chen, L., & Xing, B. (2015). Investigating the mechanisms of biochar's removal of lead from solution. *Bioresources Technology, 177*, 308–317. https://doi.org/10.1016/j.biortech.2014.11.077

Wu, L., Liu, X., Lv, G., Zhu, R., Tian, L., Liu, M., Li, Y., Rao, W., Liu, T., & Liao, L. (2021) Study on the adsorption properties of methyl orange by natural one-dimensional nano-mineral materials with different structures. *Scientific Reports, 11*, 10640. https://doi.org/10.1038/s41598-021-90235-1

Yu, J. X., Wang, L. Y., Chi, R. A., Zhang, Y. F., Xu, Z. G., & Guo, J. (2013). Competitive adsorption of Pb^{2+} and Cd^{2+} on magnetically modified sugarcane bagasse prepared in two simple steps. *Applied Surface Science, 268*, 163–170.

Zhang, M., Gao, B., Varnoosfaderani, S., Hebard, A., Yao, Y., & Inyang, M. (2013). Preparation and characterization of novel magnetic biochar for arsenic removal. *Bioresources Technology, 130*, 457–62. https://doi.org/10.1016/j.biortech.2012.11.132